Applied Physics B
Lasers and Optics

CrossMark

Absolute velocity measurement using three-beam spectral-domain Doppler optical coherence tomography

P. Sharma[1] · Y. Verma[1] · S. Kumar[1] · P. K. Gupta[1]

© Springer-Verlag Berlin Heidelberg 2015

Abstract We report the development of a three-beam spectral-domain Doppler optical coherence tomography setup that allows single interferometer-based measurement of absolute flow velocity. The setup makes use of galvo-based phase shifting to remove complex conjugate mirror artifact and a beam displacer in the sample arm to avoid cross talk image. The results show that the developed approach allows efficient utilization of the imaging range of the spectral-domain optical coherence tomography setup for three-beam-based velocity measurement.

1 Introduction

There exists considerable current interest in the use of optical coherence tomography (OCT) for simultaneous depth-resolved noninvasive imaging of tissue microstructures [1–4] and quantification of blood flow in tissue microvasculature. Doppler OCT (DOCT), a functional extension of OCT, utilizes the change in the frequency of the light scattered from a moving scatterer for the quantification of its flow. The ability of DOCT for simultaneous evaluation of tissue morphology and blood velocimetry can be of considerable diagnostic help in diabetic retinopathy, glaucoma as well as management of wounds [5–7]. The most widely used method to measure the Doppler shift is the phase-resolved method that relies on the measurement of the phase difference between the overlapping adjacent A-scans. A single-beam phase-resolved DOCT (PR-DOCT) measurement can provide only the axial velocity component along the beam [8, 9]. Therefore, in order to get absolute velocity using such a setup, one requires prior information on the angle between the flow direction and the incident beam (Doppler angle). This would require creating a 3D image of the sample from which the orientation of the vessel can be computed using two cross-sectional B-frames separated by a known distance [10]. However, the accuracy of the measurement of the Doppler angle is limited by the unavoidable motion artifacts in live samples. Further, the need to acquire multiple B-frames makes this approach labor-intensive and time-consuming. Several dual-beam PR-DOCT measurements have also been reported that provide the component of velocity in the plane containing two probe beams [11–13]. Absolute velocity measurement using the dual-beam approach requires aligning the plane of the two beams with the orientation of the vessel making the approach labor-intensive and time-consuming. Determination of absolute velocity in a single measurement without prior knowledge of flow direction requires the use of three or more probe beams that probe a single location in the sample from different incidence angles. Previously a three-beam spectral-domain OCT (SD-OCT) setup for absolute flow velocity measurement has been demonstrated where the images corresponding to the three beams were separated by introducing a suitable path length delay [14]. This approach severely limits the achievable imaging depth in the sample because the five images (three images corresponding to the three probe beams and two additional images corresponding to the cross-coupling paths for the three beams) need to be incorporated within the limited imaging range of the SD-OCT setup. The limitation on imaging range arises because of the limited spectral

✉ P. K. Gupta
pkgupta@rrcat.gov.in

Y. Verma
yogesh@rrcat.gov.in

1   Raja Ramanna Centre for Advanced Technology,
    Indore 452013, India

Fig. 1 Schematic of the three-beam SD-DOCT setup. *SLD* superluminescent diode, *C* collimating lens, *L* focussing lens, *GW* glass window, *FC* fiber coupler, *M, M1, M2* mirrors, *BD* beam displacer, *GP* glass plate, *GS* galvoscanner, *SPA* syringe pump assembly, *TG* transmission grating, *LSC* line-scan camera. Labels *1*, *2* and *3* represent the three probe beams
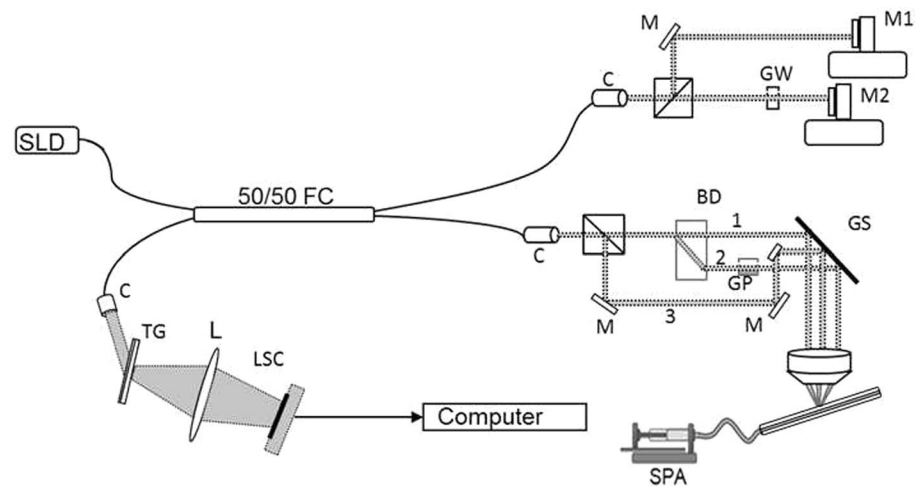
resolution of the spectrometer which results in a decrease in the contrast of interference fringes as the depth of imaging increases [15]. One approach to circumvent this problem is to make use of vertical cavity surface-emitting lasers (VCSEL) which offer a large (up to ~10 s cm) coherence length at a given instantaneous wavelength resulting in a large imaging depth [16]. Another approach is to use three separate interferometers, one for each probe beam in the spectral-domain optical coherence tomography setup [17]. However, the use of three sources and three spectrometers not only results in higher cost but makes the system rather complex and alignment sensitive.

In this paper, we report the development of a three-beam spectral-domain Doppler optical coherence tomography (SD-DOCT) setup that allows measurement of absolute velocity using a single B-frame without prior knowledge of vessel orientation. In order to avoid cross talk image that limits the achievable depth range, we make use of a beam displacer in the sample arm to generate two orthogonal polarization beams and a galvoscanner-based phase shifting to remove complex conjugate mirror artifact.

2 System description

A schematic of the phase-resolved SD-DOCT setup for absolute velocity measurement is shown in Fig. 1. A 15-mW superluminescent diode source with center wavelength 840 and 40 nm bandwidth was used to illuminate a 50:50 single-mode fiber-based Michelson interferometer. In the sample arm, a nonpolarizing beam splitter was used to split the beam into two parts. One of these beams was further split using a beam displacer (BD) into two linear orthogonally polarized parallel beams with ~4 mm spatial shift between them. The horizontally polarized beam labeled as '1' emerged straight, while the vertically polarized beam labeled as '2' emerged at a spatial offset of 4 mm. The third beam labeled as '3' was also diverted to the galvoscanner using a pair of additional mirrors. A glass plate (GP) was inserted in the beam path of vertically polarized probe beam to match the optical path of the probe beams 1 and 2. The optical path of probe beam 3 was adjusted such that the optical path delay between probe beams 3 and 1 (or 2) was at least twice the imaging range of the setup. Such a large optical path difference was chosen so that any cross-coupling between probe beams 3 and 1(or 2) does not contribute to interference signal. These three beams were made to fall on the galvoscanner such that they formed the three vertices of an equilateral triangle (side ~4 mm), which were located away from the pivot axis of the galvoscanner. After reflecting from the galvoscanner, these three beams were focussed to a common spot on the sample using a lens of focal length 50 mm. This resulted in an angle of ~4.5° between the probe beams. Although the NA of the lens was 0.25, the effective NA in our setup was ~0.012 because the lens aperture was under-filled (beam size ~1.2 mm) to achieve large depth of focus and to allow beam steering at lens aperture for performing lateral scan.

Figure 2 shows the (a) top (*XY* plane) and (b) side views of the geometry of the probe beams focusing at the sample. Here α_1, α_2 and α_3 are the angles between three probe beams and the tube, *v* is flow velocity vector, and v_1, v_2 and v_3 are the velocity components along the three probe beams.

In the reference arm, another nonpolarizing beam splitter was used to split the beam into two reference beams. One reference beam was path-matched to probe beams 1 and 2, while the other was path-matched to probe beam 3. A glass window (GW) of appropriate thickness was incorporated in the reference arm (for probe beams 1 and 2) to minimize the dispersion mismatch arising due to the use of BD in generation of probe beams 1 and 2. The light beams

Fig. 2 Focusing geometry of three probe beams **a** *top view* and **b** *side view*
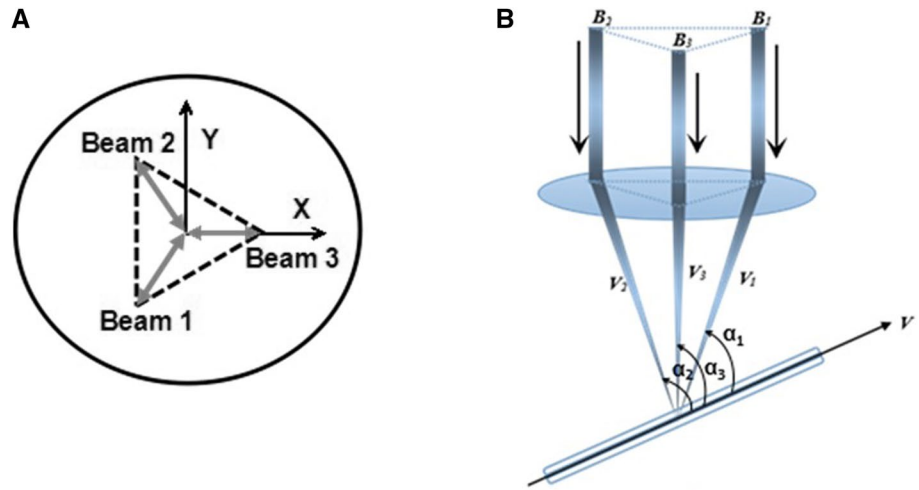
reflected from the reference and the sample arms recombine and generate interference fringes. These delay-encoded interference patterns were detected by a custom-made spectrometer comprising of a collimating lens (focal length 5 cm), a volume-phase holographic transmission grating with 1200 lines/mm, a focussing lens of focal length 15 cm and a line-scan camera (Atmel Aviiva, 1024 pixels) operating at 10 kHz line rate [12, 18]. These interference spectra were first processed with background subtraction, re-sampling in k-space, and then Fourier-transformed to generate the depth-resolved intensity and phase images. Further, the phase images corresponding to the three probe beams were also corrected for the phase shift introduced by the galvoscanner. The axial and lateral resolutions of the three-beam SD-DOCT setup were ~10 and ~50 μm, respectively. The maximum imaging range was ~4 mm, limited by the spectral resolution (~0.1 nm) of the spectrometer. The sensitivity roll-off value for the system was ~3 dB for 1-mm optical delay. The measured sensitivity (SNR) of the system was 90, 91 and 88 dB for the probe beams 1, 2 and 3, respectively.

3 Methodology

To avoid the overlap of the OCT images corresponding to the three probe beams, the images need to be separated in optical path. To achieve this, the galvoscanner-induced phase shifting method [19] was incorporated, which removes the complex conjugate artifacts and doubles the imaging range of the system. The sample arm of the system was aligned such that the probe beams 1 and 3 are reflected from one side of the pivot axis of the galvoscanner, while probe beam 2 was reflected from other side of the pivot axis. The phase shifts introduced in each of the three beams during lateral scanning can be used to remove the complex conjugate artifact. Hilbert transformation (for a given k along time or X-axis) and then Fourier transformation along k-axis place the images corresponding to probe beams 1 and 3 on one side of the zero-delay line, while the image for probe beam 2 on opposite side of zero-delay line. The optical paths of probe beams 1 and 2 were adjusted such that the corresponding images are placed at equal distances on opposite side of the zero-delay line in depth domain. The advantage of this scheme is that depth-dependent sensitivity variation for the two probe beams (1 and 2) becomes identical. Also the reduction in sensitivity for probe beam 3 due to depth-dependent sensitivity decay in FD-OCT was partly compensated by an increase in the power for probe beam 3. The BD used to generate two orthogonal polarization probe beams (1 and 2) helps avoid the cross talk image [12]. The optical path of the third probe beam was adjusted such that the corresponding image was separated from the orthogonal polarization images by a distance greater than the achievable imaging depth of the setup. Since the three probe beams make different angles of incidence ($\alpha_{1,2,3}$) with the flow direction, phase difference measurements ($d\Phi_{1,2,3}$) for each of the phase images provide the corresponding axial velocity components ($v_{1,2,3}$). By making use of the axial velocity components, the three velocity components ($v_{x,y,z}$) and absolute velocity were determined using the following equations [17]:

$$v_1 = e_{1x} \cdot v_x + e_{1y} \cdot v_y + e_{1z} \cdot v_z = d\varphi_1 \frac{\lambda}{4\pi \Delta T n \cos \alpha_1} \quad (1)$$

$$v_2 = e_{2x} \cdot v_x + e_{2y} \cdot v_y + e_{2z} \cdot v_z = d\varphi_2 \frac{\lambda}{4\pi \Delta T n \cos \alpha_2} \quad (2)$$

$$v_3 = e_{3x} \cdot v_x + e_{3y} \cdot v_y + e_{3z} \cdot v_z = d\varphi_3 \frac{\lambda}{4\pi \Delta T n \cos \alpha_3} \quad (3)$$

Fig. 3 **a** Intensity, **b** phase images for the three probe beams and **c** axial velocity distributions along each probe beam. *X* and *Z* denote the lateral and axial dimensions, respectively. Solid *circles* and *line* represent experimental data and its parabolic fit, respectively
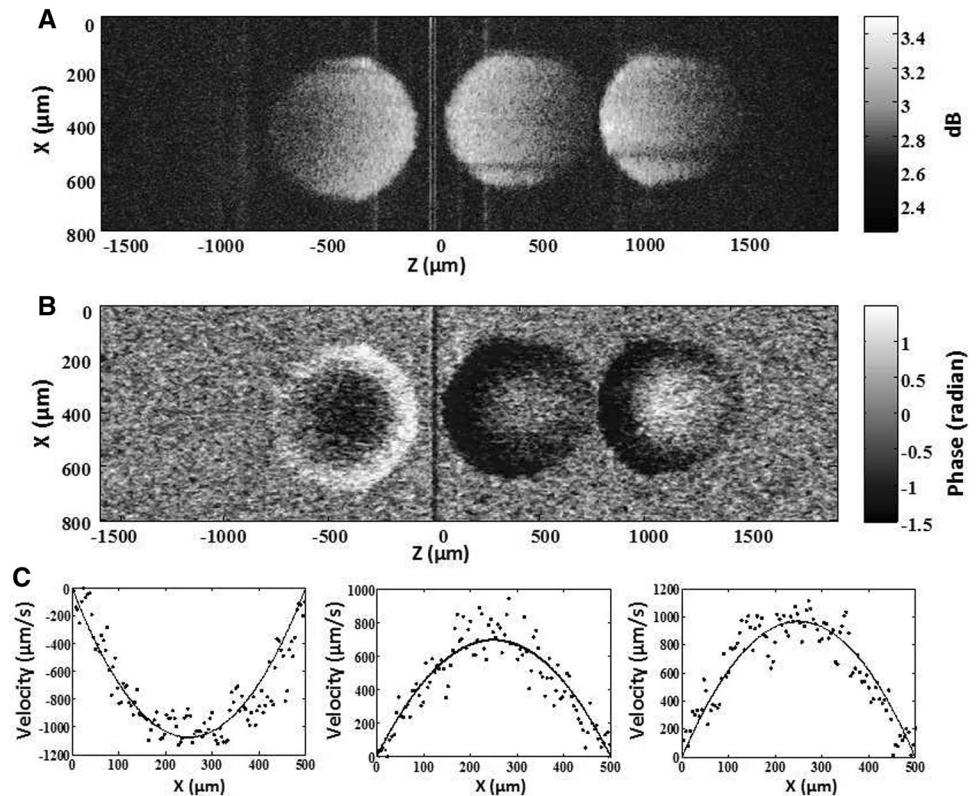
4 Results

In order to validate the scheme, absolute velocity measurements were carried out on a tissue phantom flowing through a glass tube. A syringe pump was used to flow 1 % Intralipid solution in water through a glass tube of 0.5 mm inner diameter with velocity varying from ~1.5 to 9 mm/s. Taking account of the facts that most often blood vessels are oriented roughly parallel to the tissue surface [20] and that the Doppler measurements get increasingly inaccurate as Doppler angle approaches 90°, for validation of our scheme we performed experiments for Doppler angles in the range of 60°–70°. Figure 3 shows the measured intensity and phase images obtained for the

flowing Intralipid solution with glass tube oriented at an angle of 70° with respect to *Z*-axis. Axial velocity components v_1, v_2 and v_3 were calculated by parabolic fitting of the measured velocity profiles. These axial velocity components were used to calculate the flow velocity components v_x, v_y and v_z along *X*-, *Y*- and *Z*-axis using Eqs. 1–3. The measured as well as fitted axial velocity distribution profiles for the three probe beams are shown in Fig. 3c. The measured velocity profiles are an average over ten consecutive A-scans which provides experimentally measured velocity ~7.8 mm/s for the set velocity of 8.5 mm/s.

In Fig. 4a, we show the experimentally measured flow velocities for the same orientation of the glass tube for

Fig. 4 **a** Absolute velocity measurement for different set velocities for a constant tilt angle of tube **b** absolute velocity measurement for different tilt angles of the glass tube
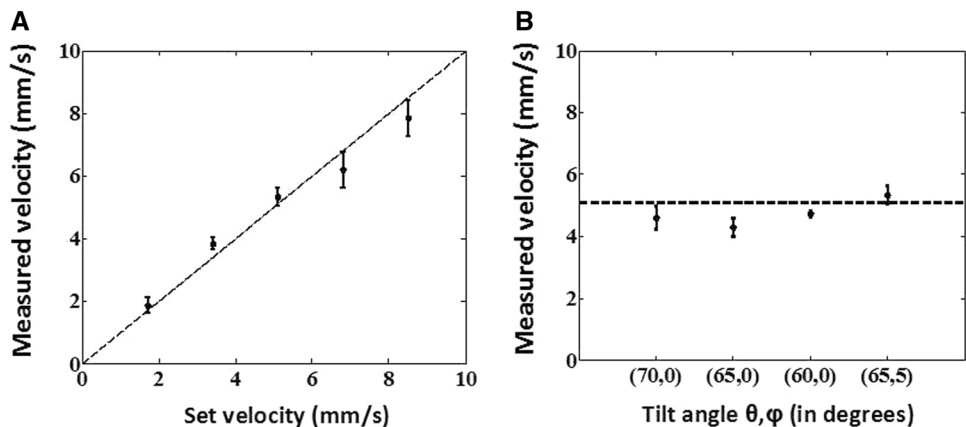
different flow velocities set by syringe pump. Good agreement can be seen between set and measured velocities. Figure 4b shows the velocity measurements carried out for different tilt angles of the glass tube with respect to Z-axis (θ) and X-axis (φ). The measured flow velocity 4.7 ± 0.4 mm/s for these different orientations of glass tube matches reasonably with the set flow velocity of 5.1 mm/s. The dotted line and solid circle show the expected and measured values, and the error bars equal the standard deviation of the measured velocity values. The deviation between the set and measured velocities could be due to the refraction of the probe beams at the outer surface of the glass tube.

5 Conclusion

To conclude, we have developed a three-beam single-detector SD-DOCT setup that allows measurement of absolute velocity using a single B scan without prior knowledge of vessel orientation. The use of phase shifting introduced by the galvoscanner to remove the complex conjugate mirror artifact and the use of beam displacer in the sample arm of the fiber-optic interferometer to generate orthogonal polarization beams allow efficient utilization of the achievable depth range and measurement sensitivity of the SDOCT setup for velocity measurement without any cross talk. The approach has been validated by measurement of flow velocity in a flow phantom.

References

1. D. Huang, E.A. Swanson, C.P. Lin, J.S. Schuman, W.G. Stinson, W. Chang, M.R. Hee, T. Flotte, K. Gregory, C.A. Puliafito, J.G. Fujimoto, Science **254**, 1178–1181 (1991)
2. F. Fercher, W. Drexler, C.K. Hitzenberger, T. Lasser, Rep. Prog. Phys. **66**, 239 (2003)
3. D. Stifter, Appl. Phys. B **88**, 337–357 (2007)
4. Y. Verma, K.D. Rao, M.K. Suresh, H.S. Patel, P.K. Gupta, Appl. Phys. B **87**, 607–610 (2007)
5. S.M. Daly, M.J. Leahy, J. Biophotonics **6**, 217–255 (2013)
6. J. Flammer, S. Orgül, V.P. Costa, N. Orzalesi, G.K. Krieglstein, L.M. Serra, J.P. Renard, E. Stefánsson, Prog. Retinal Eye Res. **21**, 359 (2002)
7. B. Pemp, L. Schmetterer, J. Can. Ophthalmol. **43**, 295 (2008)
8. B.J. Vakoc, S.H. Yun, J.F. de Boer, G.J. Tearney, B.E. Bouma, Opt. Express **13**, 5483 (2005)
9. Y. Zhao, Z. Chen, C. Saxer, S. Xiang, J.F. de Boer, J.S. Nelson, Opt. Lett. **25**, 114–116 (2000)
10. Y. Wang, B.A. Bower, J.A. Izatt, O. Tan, D. Huang, J. Biomed. Opt. **12**, 041215 (2007)
11. N.V. Iftimia, D.X. Hammer, R.D. Ferguson, M. Mujat, D. Vu, A.A. Ferrante, Opt. Express **16**, 13624 (2008)
12. S. Kumar, Y. Verma, P. Sharma, R. Shrimali, P.K. Gupta, Appl. Phys. B **117**, 395 (2014)
13. R.M. Werkmeister, N. Dragostinoff, M. Pircher, E. Gotzinger, C.K. Hitzenberger, R.A. Leitgeb, L. Schmetterer, Opt. Lett. **24**, 2967–2969 (2008)
14. Y.C. Ahn, W. Jung, Z. Chen, Opt. Lett. **32**, 1587 (2007)
15. J. Ai, L.V. Wang, Appl. Phys. Lett. **88**, 111115 (2006)
16. I. Grulkowski, J.J. Liu, B. Potsaid, V. Jayaraman, C.D. Lu, J. Jiang, A.E. Cable, J.S. Duker, J.G. Fujimoto, Biomed. Opt. Express **3**, 2733–2751 (2012)
17. W. Trasischker, R.M. Werkmeister, S. Zotter, B. Baumann, T. Torzicky, M. Pircher, C.K. Hitzenberger, J. Biomed. Opt. **18**, 116010 (2013)
18. Y. Verma, P. Nandi, K.D. Rao, M. Sharma, P.K. Gupta, App. Opt. **50**, E7 (2011)
19. L. An, R.K. Wang, Opt. Lett. **32**, 3423–3425 (2007)
20. C. Blatter, S. Coquoz, B. Grajciar, A.S.G. Singh, M. Bonesi, R.M. Werkmeister, L. Schmetterer, R.A. Leitgeb, Biomed. Opt. Express **4**, 1188–1203 (2013)